

Article

Low-Speed DSMC Simulations of Hotwire Anemometers at High-Altitude Conditions

Christopher A. Roseman ^{*}  and Brian M. Argrow 

Smead Aerospace Engineering Sciences, University of Colorado Boulder, Boulder, CO 80303, USA;

Brian.Argrow@colorado.edu

* Correspondence: Christopher.Roseman@colorado.edu

Abstract: Numerical simulations of hotwire anemometers in low-speed, high-altitude conditions have been carried out using the direct simulation Monte Carlo (DSMC) method. Hotwire instruments are commonly used for in-situ turbulence measurements because of their ability to obtain high spatial and temporal resolution data. Fast time responses are achieved by the wires having small diameters (1–5 μm). Hotwire instruments are currently being used to make in-situ measurements of high-altitude turbulence (20–40 km). At these altitudes, hotwires experience Knudsen number values that lie in the transition-regime between slip-flow and free-molecular flow. This article expands the current knowledge of hotwire anemometers by investigating their behavior in the transition-regime. Challenges involved with simulating hotwires at high Knudsen number and low Reynolds number conditions are discussed. The ability of the DSMC method to simulate hotwires from the free-molecular to slip-flow regimes is demonstrated. Dependence of heat transfer on surface accommodation coefficient is explored and discussed. Simulation results of Nusselt number dependence on Reynolds number show good agreement with experimental data. Magnitude discrepancies are attributed to differences between simulation and experimental conditions, while discrepancies in trend are attributed to finite simulation domain size.

Keywords: DSMC; rarefied; transition-regime; hotwire; Nusselt number; calibration; low-speed; Reynolds number



Citation: Roseman, C.A.; Argrow, B.M. Low-Speed DSMC Simulations of Hotwire Anemometers at High-Altitude Conditions. *Fluids* **2021**, *6*, 20. <https://doi.org/10.3390/fluids6010020>

Received: 1 December 2020

Accepted: 28 December 2020

Published: 2 January 2021

Publisher's Note: MDPI stays neutral with regard to jurisdictional claims in published maps and institutional affiliations.



Copyright: © 2021 by the authors. Licensee MDPI, Basel, Switzerland. This article is an open access article distributed under the terms and conditions of the Creative Commons Attribution (CC BY) license (<https://creativecommons.org/licenses/by/4.0/>).

1. Introduction

Recent demand for hypersonic vehicles requires an increased understanding of turbulence in the stratosphere, the region of the atmosphere in which these vehicles will likely cruise. The Hypersonic Flight in the Turbulent Stratosphere (HYFLITS) research campaign, supported by the Air Force Office of Scientific Research (AFOSR) Multidisciplinary University Research Initiative (MURI), is making in-situ measurements of stratospheric turbulence with balloon-borne hotwire anemometers. Hotwires have long been used to measure turbulent fluctuations of velocity. Calibration of these anemometers is a crucial step in this research effort. The balloon-borne instruments will experience mean flow rates between 1 and 10 m/s. Corresponding hotwire Reynolds number (Re) values at the altitudes of interest have a wide range, $1.2 \times 10^{-3} < Re < 3.1 \times 10^{-1}$. Low air density in the stratosphere results in fine-wire Knudsen number values ($Kn = \lambda/d$, where λ is the mean free path) in the range $0.1 < Kn < 4$ based on a wire diameter of $d = 5 \mu\text{m}$. These values correspond to the transition-regime between slip-flow and free-molecular flow. Extensive theoretical and experimental studies have been conducted for hotwires in the continuum ($Kn < 10^{-3}$) and slip-flow ($10^{-3} < Kn < 10^{-1}$) regimes [1–5]. Little work has been published that addresses the behavior of hotwires in the transition-regime ($10^{-1} < Kn < 10^1$) [6,7].

The seminal work for hotwire instruments is that of King [1] who first derived a relationship (known as King's law) between wire energy transfer and streaming velocity. King's law can be expressed in non-dimensional form as

$$\text{Nu} = \tilde{A} + \tilde{B}\text{Re}^n. \quad (1)$$

Re is the wire Reynolds number given by

$$\text{Re} = \frac{\rho U_\infty d}{\mu} \quad (2)$$

where ρ is the fluid density, μ is the fluid dynamic viscosity, and U_∞ is the free-stream fluid velocity. Nusselt number, Nu, is the non-dimensional ratio of the convective and conductive energy transfer from the wire and is given by

$$\text{Nu} = \frac{hd}{k} \quad (3)$$

where k is the thermal conductivity of the fluid and h is the convective heat transfer coefficient,

$$h = \frac{Q}{A(T_w - T_\infty)}. \quad (4)$$

In Equation (4), Q is the heat transfer from the wire surface to the surrounding fluid, T_w is the wire temperature, T_∞ is the free-stream gas temperature, and A is the surface area of the wire. In equation [1], the values for \tilde{A} , \tilde{B} , and n are determined by experimental calibration. The original derivation of King [1] suggested a value of 0.5 for n . This has been shown to be fairly accurate for $\text{Re} \gtrsim 44$, the value at which vortex-shedding commences [2]. Collis and Williams [2] experimentally investigate hotwires in low Reynolds number flows. They propose a slightly different calibration law that includes an explicit dependence on the film and free-stream temperatures:

$$\text{Nu} \left(\frac{T_f}{T_\infty} \right)^{-0.17} = \tilde{A} + \tilde{B}\text{Re}^n. \quad (5)$$

Values for \tilde{A} , \tilde{B} , and n are different depending on whether Re is above or below the value at which vortex shedding occurs. The temperature ratio is included as a way of taking into account the fact that fluid properties are a function of temperature.

An experimental study by Andrews et al. [5] explores the dependence of Nu on Kn. Experimental results are presented for Kn values up to about 0.1. The relationship they propose has the same form as Equation (1) with $\tilde{A} = 0.34$, $\tilde{B} = 0.65$, and $n = 0.45$. The value for Nu given by Equation (1) with the provided constants is referred to as the continuum Nusselt number. This value of Nu differs from the measured value, Nu_m , because of the thermal slip at the wire surface when wire Kn is in the slip-flow regime. A correction to the continuum Nu to obtain the measured Nusselt number Nu_m is given as

$$\text{Nu} = \frac{\text{Nu}_m}{1 - \phi \text{Kn} \text{Nu}_m}. \quad (6)$$

Equation (6) is derived from kinetic theory and a first-order approximation of the temperature-jump boundary condition. The value for ϕ depends on the accommodation coefficient at the surface of the wire. A value of $\phi = 2$ successfully captured the slip effects seen in the experimental data of Andrews et al. [5]. Equation (6) was also presented in Collis and Williams [2], though they did not have enough experimental data to thoroughly expound upon its validity. A similar expression was derived in the extensive theoretical study of Kassoy [4].

Equation (6) is limited by the fact that its derivation depends on a first-order approximation of the thermal slip at the wire surface [8]. This assumption degrades at higher Kn values because property gradients are no longer linear over a distance approximately equal to the mean free path. Second-order slip boundary conditions were derived by Deissler [8]. Although these boundary conditions have not been used to derive solutions for hotwire heat transfer, they show only a slight improvement over first-order boundary conditions in terms of the applicable range of Kn.

An experimental study by Xie et al. [6] presents hotwire heat transfer results in the transition-regime and velocities between 0.5 and 20 m/s ($10^{-3} < \text{Kn} < 3$, $10^{-3} < \text{Re} < 20$). Their results show a clear decrease in Nu with increasing Kn. They present an empirical correlation for Nu as a function of Re and Kn:

$$\text{Nu} = \tilde{A} + \tilde{B}\text{Re}^n + \tilde{C}\text{Kn}^m + \tilde{D}\text{Re}^i\text{Kn}^j. \quad (7)$$

Values for the constants in Equation (7) are calculated using a non-linear least-squares fit to the experimental data. No physical justification was given for Equation (7). Data published by Xie et al. [6] and a subsequent study by the same group are the only transition-regime hotwire experimental results that the authors are aware of [7].

Few numerical simulation investigations of fine-wire heat transfer have been conducted [7,9–12]. Çelenligil [12] uses the direct simulation Monte Carlo (DSMC) method to explore heat transfer to cylinders with Kn = 0.02 and 0.2. Cylinder Re ranged from 0.6 to 24. In Xie et al. [7], slip-flow boundary conditions are derived and implemented into the ANSYS Fluent finite volume computational fluid dynamics (CFD) solver. The study is limited to low wire temperatures relative to the free-stream ($T_w - T_\infty \approx 1^\circ\text{C}$) to avoid implementing temperature-dependent fluid properties. At Kn < 0.1, simulation results show good agreement with selected experimental data from Xie et al. [6] and with several published Nu correlations including Collis and Williams [2]. Numerical results diverge significantly from experiment for Kn > 0.1.

This article addresses the simulation of hotwire instruments in the transition-regime. An understanding of this flow regime is crucial for using these instruments to make in-situ stratospheric turbulence measurements. Numerical simulations are performed using the DSMC method. Details of the simulation methodology are described in Section 2. A comparison between simulation results, published experimental data, and free-molecular theory is presented in Section 3. Finally, Section 4 summarizes the main conclusions from the current study.

2. Numerical Simulation Methodology

Continuum CFD models fail in the transition-regime from slip-flow to rarefied-flow where $10^{-1} \leq \text{Kn} \leq 10^1$ because particle collisions are infrequent enough that gases cannot be treated as a continuous media, but particle collisions are frequent enough that they cannot be ignored as is done in free-molecular theory. The DSMC method was pioneered by Graeme Bird for modeling flows from the transition to free-molecular regimes [13].

The current study utilizes the open source DSMC code SPARTA developed by Sandia National Laboratory (Stochastic PARallel Rarefied-gas Time-accurate Analyzer, <http://sparta.sandia.gov>) [14]. The variable soft sphere model was used to model particle collisions. Internal rotational energy is modeled, and vibrational energy is ignored. SPARTA uses the no time counter algorithm for selecting collision partners. The Larsen-Borgnakke model is used with a constant rotational relaxation number to model the exchange of rotational and translational energy during collisions. Table 1 provides the parameters for collision models used for the two different gas species simulated in the current study.

Table 1. Parameters for the variable soft sphere collision model and the Larsen-Borgnakke model used in the current study. σ_c is the collision diameter, ω is the temperature exponent for viscosity, T_{ref} is the reference temperature, α_s is the angular scattering parameter, ζ_{rot} is the number of rotational degrees of freedom, and Z_{rot} is the rotational relaxation number.

Gas Species	$\sigma_c \times 10^{10}$, m	ω	T_{ref} , K	α_s	ζ_{rot}	$1/Z_{rot}$
Nitrogen, N ₂	4.07	0.74	273.15	1.6	2	0.2
Oxygen, O ₂	3.96	0.77	273.15	1.4	2	0.2

Present simulations predict heat flux Q to the surface of a heated wire. Heat transfer results are reported as non-dimensional Nusselt number values (Equation (3)) with thermal conductivity k evaluated at the film temperature T_f , equal to the arithmetic mean of the wire and free-stream temperatures. An f subscript on the symbols for non-dimensional numbers (Re_f , Nu_f , Kn_f) indicate that the value was calculated using fluid properties evaluated at T_f (k_f , μ_f , ρ_f , λ_f). Fluid conductivity k_f and viscosity μ_f are calculated using equations from the 1976 Standard Atmosphere [15]. Density is calculated using the ideal gas law

$$\rho_f = \frac{P}{R_{gas}T_f} \quad (8)$$

where P is pressure and R_{gas} is the specific gas constant. Mean free path λ_f is calculated by

$$\lambda_f = \frac{\sqrt{2}RT_f}{2\pi A_v(3.65 \times 10^{-10})^2P} \quad (9)$$

where R is the universal gas constant and A_v is Avogadro's number [15].

To date, the DSMC method has primarily been used for the simulation of rarefied supersonic flows. Common applications include satellites [16], reentry vehicles [17], and microelectromechanical systems [18]. A number of studies have used DSMC to study subsonic flows through channels or porous materials [19–28]. Fewer studies have investigated subsonic, external aerodynamic flows around a body [12,29–31]. The current study simulates heated circular cylinders with infinite length at very low Reynolds number values. Challenges associated with simulating low-speed, external aerodynamic flows are discussed below.

2.1. Statistical Scatter

Subsonic, low-speed DSMC simulations suffer from large statistical scatter because the method stochastically models particle thermal velocities which are typically ~ 300 m/s. Several researchers have demonstrated so-called information preservation (IP) methods that reduce statistical scatter for low-speed DSMC [19,21]. These methods have not been implemented into the SPARTA DSMC code. The current study addresses the problem of statistical scatter by taking large numbers of samples at steady-state conditions. This later approach comes at a much higher computational cost than IP methods, though with increasing efficiency and power of computers the cost is manageable with an available supercomputer resource. Figure 1 shows a representative case for how hotwire heat transfer changes as a simulation progresses. The orange line spans the steady-state section of data and shows the average and standard deviation (σ) of those data.

To clarify the DSMC results presented in this study, a detailed description of the averaging and sampling procedures is warranted. During a DSMC simulation, numerical particles are moved throughout the domain and collide with one another in a stochastic manner. During the course of a simulation, SPARTA allows for data to be continually averaged and dumped every N time-steps. The information of interest to the current study is the energy transfer between the wire surface and the gas. Each data point in Figure 1 represents the average heat transfer to the surface for the previous N time-steps. Lower values of N (higher sampling frequency) will result in larger scatter in the output data than

if a larger value of N is used (lower sampling frequency). For larger values of N , larger data sets are averaged for each output data point which effectively filters out the high-frequency, random fluctuations in the wire heat transfer rate. Fluctuations are filtered out more with increasing N . Preliminary simulations were run with a sampling frequency of $N = 1000$ to establish a clear understanding of the time-variation of the heat transfer. After these preliminary simulations, most production simulations were run with a decreased sampling frequency ($N = 10,000$). Small sampling frequencies (large N) are desired to speed up simulation run times, reduce memory required to store the output data, and to reduce post-processing time.

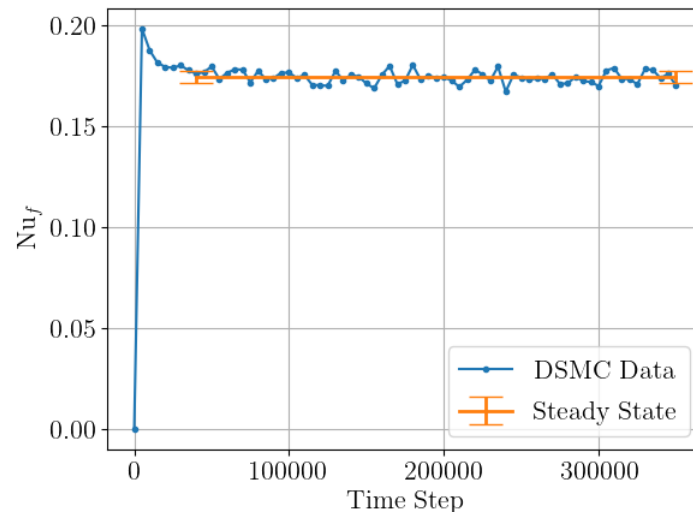


Figure 1. Typical time dependent result for wire heat transfer for hotwire direct simulation Monte Carlo (DSMC) simulations. The solid orange line shows the average of the steady-state data and $\pm 1\sigma$.

It should be noted that the dump frequency will not change the calculated average of the steady-state data, only the scatter of those data (visualized by σ). This is because each output data point represents the average of an equal number of per-time-step data points. An average of the averaged per-time-step data will be equal to the average of the original set of data. DSMC results throughout this study are presented as a point with error bars. The point represents the average of the steady-state data, and the error bars indicate $\pm 1\sigma$ of the output data.

A simple algorithm was used to determine the section of steady-state data from the time-history data like that shown in Figure 1. The algorithm follows the process enumerated below.

1. Select entire time series of heat transfer data (t, Nu_f) as initial window of data
2. Normalize the time t in the window of data to have a range between 0 and 1 ($0 \leq t^* \leq 1$)
3. Calculate the average Nu_f in the data window ($\overline{Nu_f}$)
4. Express Nu_f values as a percent change from the window average:

$$Nu_f^* = 100 \times \frac{Nu_f - \overline{Nu_f}}{\overline{Nu_f}}$$
5. Perform a linear regression analysis of the normalized data (t^*, Nu_f^*)
6. Compare the slope of the linear fit $d\overline{Nu_f}/dt^*$ to the tolerance value of 1:
 - (a) If $d\overline{Nu_f}/dt^* \geq 1$: remove first data point (where $t^* = 0$) from the current window of data and repeat steps 2–6
 - (b) If $d\overline{Nu_f}/dt^* < 1$: current window is the estimated steady-state section of data and the process ends

After the algorithm is completed, plots like the one shown in Figure 1 are produced and visually inspected to check that the algorithm chose a reasonable set of steady-state

data. Effectively, the algorithm selects a set of data where a fitted line through that data does not predict more than 1% deviation from the data mean. Improvements can be made to increase confidence in the algorithm and eliminate the need for visual inspection. This algorithm worked well for simulations of the current study where all time-history data followed a similar trend and were well-behaved.

2.2. Boundary Conditions

Supersonic DSMC simulations typically use open (stream) and vacuum boundary conditions for domain inlets and outlets, respectively. At an open boundary, emission of particles into the domain is based on the Maxwellian thermal-velocity distribution and the free-stream velocity. Particles impacting open boundaries from inside the domain are free to leave the domain. Open boundary conditions are appropriate for any flow speed as long as the boundary is sufficiently far from the body being simulated such that its presence does not significantly change the flow conditions at the boundary. For supersonic flows, open boundaries can be placed just upstream of the bow shock wave. The location of open inlet boundary conditions is less simple for low-speed simulations because information can propagate far upstream. Domain size for low-speed DSMC is discussed later.

Vacuum boundaries do not emit particles into the domain, and all particles that impact the boundary freely leave the domain. In supersonic flows, the average streaming flow speed is much faster than the average thermal speed of particles, so particles would rarely, if ever, enter the domain through the outlet boundary. Vacuum boundary conditions are rarely appropriate for subsonic outlet boundaries where mean flow speeds are much less than the average thermal speed of particles. Low average speeds of subsonic flows means that the flux of particles into the domain from outlet boundaries must be considered to produce accurate results. Open boundary conditions for subsonic outlets are also inappropriate because the exact conditions at the outlet are often unknown. Several studies have developed and implemented implicit subsonic boundary conditions [19–21,32–34]. These methods use the flow properties of particles adjacent to the boundary to calculate the properties and number-flux of particles into the domain. This is typically applied every time-step on a per-collision-cell basis to each collision cell on a given boundary. Because collision cells contain a relatively small number of simulated particles (~ 10 , discussed below), instantaneous per-cell properties can experience large fluctuations. These fluctuations become especially significant as the streaming velocity approaches zero. Implicit boundaries can become “unstable” if a cell experiences a significant fluctuation that leads to an unrealistic emission of particles into the domain. This instability can be avoided by using implicit boundary conditions along with IP methods to reduce the statistical scatter of per-collision cell quantities [19]. Because the SPARTA DSMC code does not have IP methods, and the mean flow speeds of the current simulation are so low, implicit boundary conditions are not used in the current study. Instead, a piston boundary condition is used for the domain outlet (Chapter 12 of Bird [13]). A piston boundary is modeled as a wall moving at a specified velocity that is perpendicular to the wall face. Particles specularly reflect off of the wall. The original use of this condition was for the downstream outlet of a one-dimensional shock simulation. This condition effectively fixes the flow velocity component that is perpendicular to the wall, but it does not restrict thermal temperature or density at the boundary. Piston boundaries are less rigid than open boundary conditions where all properties are set, but they are more rigid than implicit boundaries where only pressure is specified. Piston boundary conditions are most appropriate for one-dimensional flows because (for SPARTA) wall velocity must be perpendicular to the boundary face. The current application is not one-dimensional, but vertical velocity is negligible when the outlet boundary is placed far downstream of the wire.

Preliminary simulations were run to compare open and piston outlet boundaries. Figure 2 compares the simulated temperature distribution when using piston (left) and open (right) boundary conditions at the outlet. Inlet, top, and bottom boundaries are all open at free-stream conditions. The open outlet appears to distort the thermal wake of

wire. This occurs because particles entering the domain at that boundary have a thermal temperature equal (statistically) to the free-stream. The piston boundary allows a more realistic temperature distribution to form around the wire, which is critical for accurately calculating heat transfer to the wire.

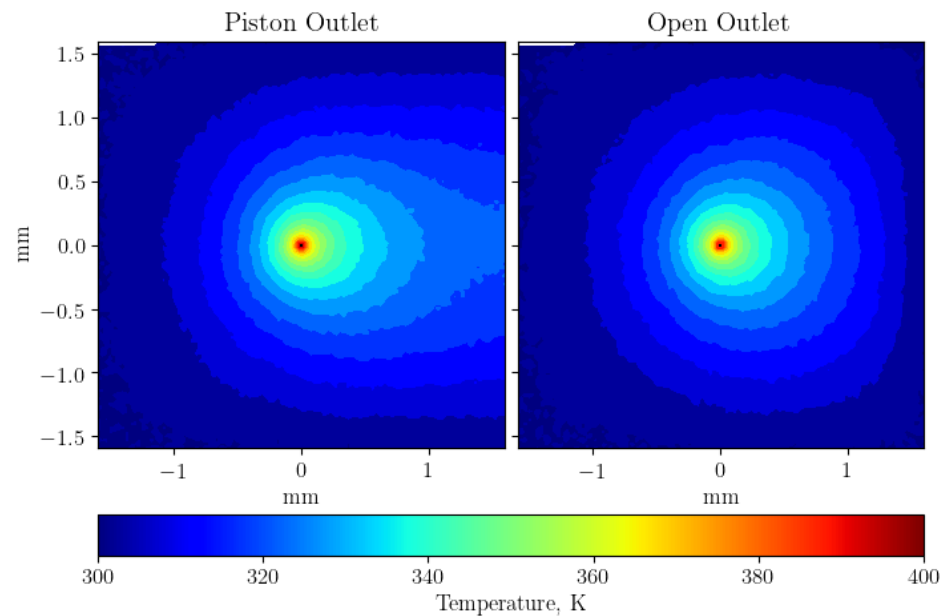


Figure 2. Simulation results for temperature distribution around the wire using a piston outlet boundary condition (left) and an open outlet boundary condition (right). All other boundaries are open.

A schematic of the domain shape and boundary conditions used for DSMC simulations in this study is shown in Figure 3. The dimension L fully defines the size of the domain which has a height of $2 \times L$ and width of $4 \times L$. The wire center is positioned $1 \times L$ downstream of the inlet and in the center of the domain vertically. Inlet, top, and bottom boundaries are treated as open with thermodynamic properties and speed set to free-stream values. A piston boundary condition is used at the outlet with the velocity equal to that of the free-stream. The domain outlet is placed far downstream of the wire in order that vertical flow at that location is negligible, and to ensure that most or all of the thermal wake of the wire is contained within the domain. Even though the speeds of interest are quite low, the results in Figure 2 show that the thermal wake extends far downstream of the wire. Optimization of the ideal downstream location of the outlet is an area for future study. Rather than simulating a half-domain with a symmetric boundary condition, the full wire was simulated. This was done in order that each simulation could provide more statistical data over which to average. Half-domain simulations were tested, but their results showed significant scatter relative to the full-domain simulations. As confidence in DSMC results for fine-wire instruments is improved with studies such as these, half-domain simulations will likely be performed in order that larger domain sizes can be used.

Collision cells were uniformly spaced in the x and y directions. Collision cell width and height L_c were set to less than half of the mean free path ($L_c \approx \lambda_f/2.1$). Simulation time-steps were set so that a particle traveling at the average thermal speed \bar{v} travels less than half a collision cell width in one time-step ($\Delta t = 0.4 L_c/\bar{v}$). Average particle thermal speed was calculated as

$$\bar{v} = \sqrt{\frac{8R_{gas}T_f}{\pi}}. \quad (10)$$

The ratio of real to simulated particles f_{num} was calculated by

$$f_{num} = \frac{n_f V_c}{N_{ppc}} \tag{11}$$

where n_f is the gas number density at T_f , V_c is the collision cell volume, and N_{ppc} is the desired number of particles per cell. Dependence of wire heat transfer on the number of simulated particles was investigated by running simulations with varying values of N_{ppc} . Results are shown in Figure 4. Free-stream velocity and temperature are 3 m/s and 300 K, respectively. Wire temperature and accommodation coefficient are 373.15 K and 0.85, respectively. Wire Kn_f is 0.65. A weak dependence on N_{ppc} is observed. Mean wire heat transfer is within 1% for all values of N_{ppc} tested. All mean values are within $\pm 1\sigma$ of the statistical scatter for the $N_{ppc} = 50$ case. Other DSMC studies of subsonic flows have used N_{ppc} values ranging from 10 to 100 [12,22,23,30,35,36]. A value of $N_{ppc} = 10$ was used for results presented in the current study. Based on the results shown, minimal error due to this relatively small number of particles is expected.

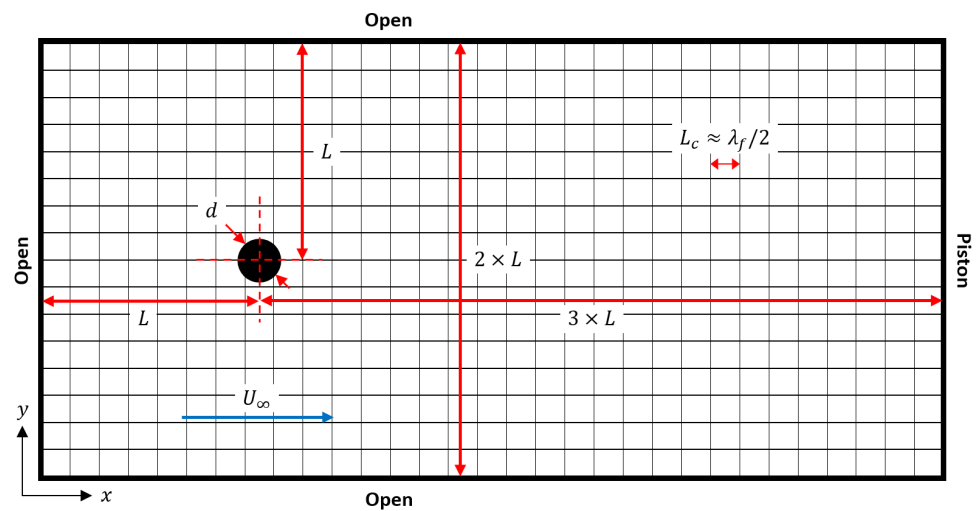


Figure 3. Schematic of the domain used for DSMC simulations. Domain size is fully defined in terms of the length L as shown. Collision cell width and height (L_c) is approximately half of the mean free path evaluated at the film temperature (λ_f).

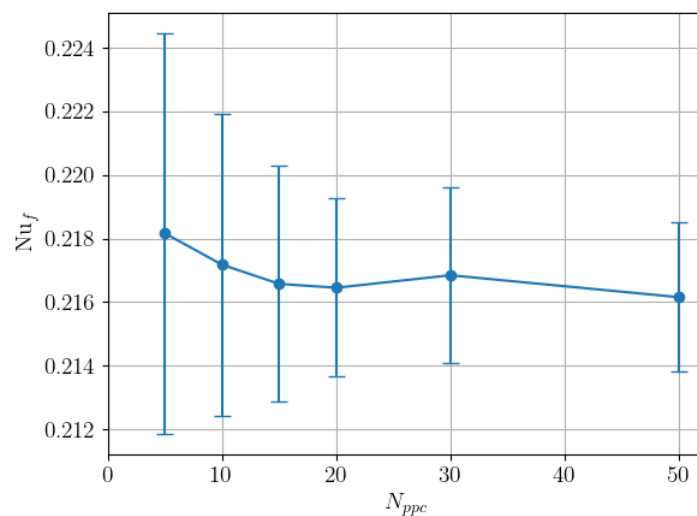


Figure 4. Dependence of wire Nusselt number on the number of simulated particles per cell. Error bars indicate $\pm 1\sigma$ of the steady-state DSMC data.

2.3. Domain Size

A typical domain size for supersonic DSMC simulations of aerodynamic flows is two or three times the size of the body in each dimension. These small domain sizes can be used because information cannot travel upstream in supersonic flows. Low-speed aerodynamic flows, especially those with high thermal gradients, need much larger domain sizes in order that the presence of the domain boundary does not influence the flow and heat transfer at the body surface. Low-speed DSMC simulations to date mostly involve micro-channel flows where the flow is physically bounded by walls, largely obviating the domain size problem that is important in external aerodynamic flows. The current study is interested in accurately estimating energy transfer from heated fine-wires, a quantity that is dependent on the temperature gradient surrounding the wire. If a simulation domain is too small, the simulation will over-predict wire heat transfer because the temperature gradient between the wall and the free-stream will be artificially increased.

Figure 5 shows the dependence of hotwire heat transfer on domain size for several conditions. The thermodynamic free-stream conditions at each altitude were calculated using the 1976 U.S. Standard Atmosphere [15]. Wire temperature T_w is set to 100 °C above the ambient for each case, and wire diameter is $d = 5 \mu\text{m}$, a typical diameter for hotwire instruments. Free-stream velocity is $U_\infty = 2, 3,$ and 2 m/s for the 25, 30, and 35 km altitude conditions, respectively. The simulated gas mixture is 20% O_2 and 80% N_2 . The Kn_f and Re_f values for the three different altitude conditions are provided in Table 2.

Table 2. Knudsen and Reynolds number values for the domain size simulations seen in Figure 5.

Altitude, km	Kn_f	Re_f
25	0.50	0.0190
30	1.08	0.0130
35	2.33	0.0039

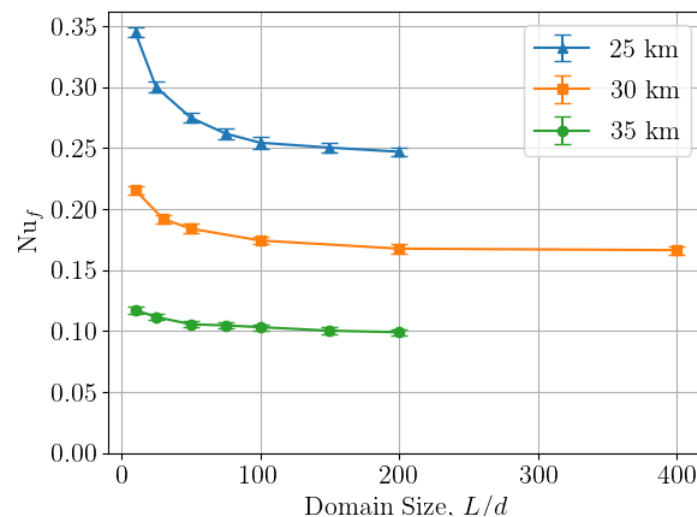


Figure 5. Dependence of hotwire heat transfer on the simulation domain size. Error bars indicate $\pm 1\sigma$ of the steady-state DSMC data.

As domain size increases, wire heat transfer should converge to a constant value for a non-zero mean flow speed. As shown, even up to $L/d = 100$, the value for Nu_f has not fully converged. Based on these results, and those of Xie et al. [7], it is expected that domain sizes of $L/d \sim 10^4$ are required to fully converge the results. At this domain size, the number of DSMC collision cells would be $\sim 10^8$, an intractably large domain size, especially for the current research interests which require large numbers of these simulations to be run. Compromising accuracy for reasonable compute times with available computational resources, a domain size of $L/d = 100$ was used for simulation results presented in this

study. Based on the results of Figure 5, the finite simulation domain will lead to an over-prediction of heat transfer by some value on the order of 10%. This bias will be lower at high Reynolds number values because convective forcing will dominate the heat transfer [7,12]. Methods to mitigate or predict the finite domain effect on results are current under investigation. Effects of finite domain size on results of the currently study are discussed below.

3. Results and Discussion

A series of hotwire DSMC simulations have been run to demonstrate the feasibility of using DSMC to accurately model hotwire heat transfer. Unless noted otherwise, all simulations performed are two-dimensional and use the domain shown in Figure 3 with $L/d = 100$.

3.1. Simulating the Transition Regime

As mentioned above, the DSMC method was primarily developed for the simulation of transition-regime flows where $10^{-1} < Kn < 10^1$. At higher Kn values, flow can be considered collisionless and free-molecular theory is valid. At lower Kn values, continuum CFD models with slip boundary conditions have been shown to accurately predict fine-wire heat transfer [7]. Figure 6 shows DSMC results for the heat transfer variation with pressure. The simulated gas is two-species air (20% O₂ and 80% N₂). Free-stream velocity is $U_\infty = 3$ m/s. Wire surface accommodation coefficient is $a_c = 0.85$, an approximate value for tungsten wires in O₂ and N₂ [37]. Free-stream and wire temperatures are 300 and 373.15 K, respectively. Also shown are experimental data from Xie et al. [7] and results for free-molecular theory [13]. The exact gas composition and temperatures for the experimental data are unclear, so a quantitative comparison with this data will not be attempted. However, simulation results agree well with the experimental data trends, thus demonstrating the feasibility of using DSMC to model hotwire heat transfer from the slip-flow regime to the free-molecular regime.

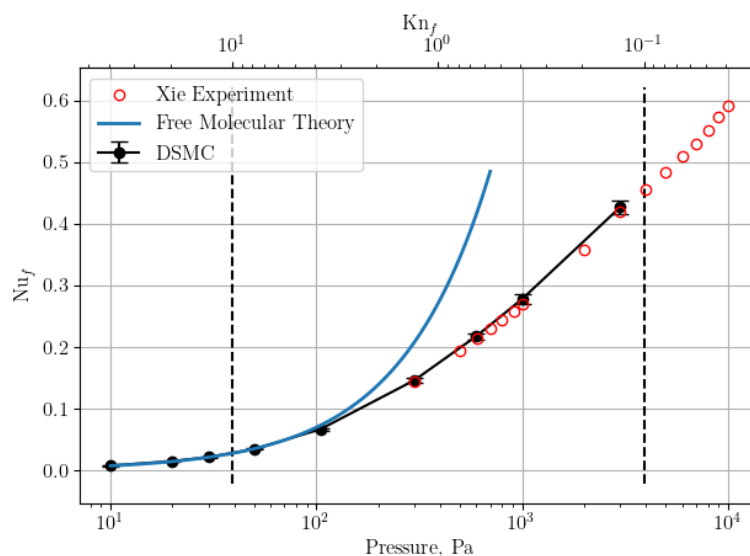


Figure 6. Comparison of free-molecular theory and experimental data to DSMC results at various pressure values (Knudsen number values). Error bars indicate $\pm 1\sigma$ of the steady-state DSMC data. Dashed vertical lines indicate the approximate Knudsen number values that define the transition-regime.

3.2. Dependence on Gas Mixture

Experimental data for hotwire anemometers has been published for a number of different gases. Two of the most common are nitrogen and air. The most relevant ex-

perimental data for the current study comes from Xie et al. [6], where nitrogen (N_2) was used. Current research efforts are focused on hotwire operation in atmospheric air. Figure 7 shows simulation results for these two different gas compositions. Air was modeled as a two-species mixture of 80% N_2 and 20% O_2 . Pressure, temperature, and velocity of simulations match experimental data from Xie et al. [6] which are also shown ($P = 1000$ Pa, $T_w = 373$ K, $T_\infty = 300$ K, $U_\infty = 1\text{--}20$ m/s). The difference between the two sets of DSMC data is $< 3\%$ (relative to air results). From these results, it can be concluded that comparisons between simulations and experiments that have slightly different gas mixtures are meaningful. Mixture independence for hotwire heat transfer has also been shown experimentally for the slip-flow regime [5]. It should be noted that the nitrogen and air mixtures are both diatomic. Further investigation is required to determine the dependence of results on the number of internal degrees of freedom of a gas mixture.

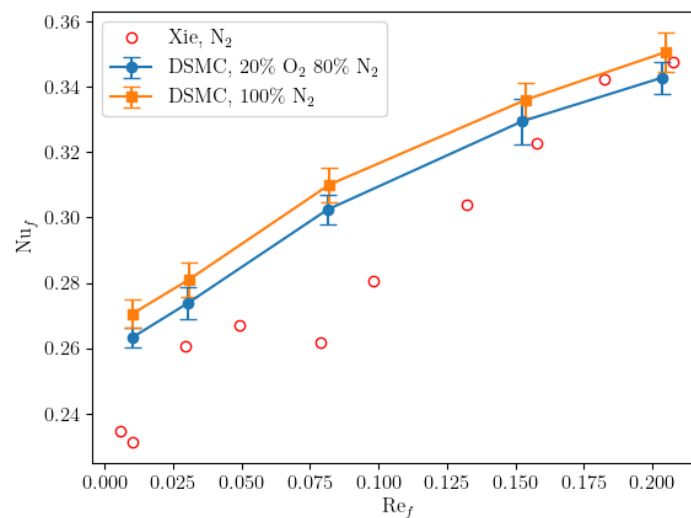


Figure 7. Comparison of DSMC simulation results using two different gas mixtures and experimental data [6]. Error bars indicate $\pm 1\sigma$ of the steady-state DSMC data.

3.3. Dependence on Accommodation Coefficient

Thermal accommodation coefficient, a_c^* , quantifies the efficiency of energy transfer between a gas and a surface. A typical definition for a_c is

$$a_c^* = \frac{q_i - q_r}{q_i - q_w} \quad (12)$$

where q_i is the incident energy flux, q_r is the energy flux of particles reflected off the surface, and q_w is the energy flux away from the surface if all reflected particles are emitted from the surface according to the Maxwellian equilibrium distribution at the wall temperature ($0 \leq a_c^* \leq 1$). Experimental determination of a_c^* can be quite difficult because it depends on many factors including the gas mixture, surface material, surface temperature, pressure, and surface manufacturing details [5,37–39]. Manufacturing inconsistencies and surface impurities can significantly change a_c^* , especially for micro-surfaces whose surface flaws have a length scale similar in magnitude to the surface itself.

A specific value for a_c^* can be modeled simply in the DSMC method by considering a mix of specular and diffuse reflections. During a specular reflection, the normal velocity of an impacting particle is reversed and internal energy modes remain unchanged. Particle energy before and after the surface reflection is equal, so no energy transfer occurs. During a diffuse reflection, a particle that impacts a surface is assumed to be absorbed, then re-emitted from the surface in a random direction with a speed and internal energy according to the Maxwellian equilibrium distribution at the surface temperature. The fraction of diffusely reflected particles is specified for a simulation by the parameter a_c . A specific

value for a_c^* is modeled by setting $a_c = a_c^*$. If $a_c = 1$, all particles are diffusely reflected and $q_r = q_w$. If $a_c = 0$, all particles are specularly reflected and $q_r = q_i$. The net energy exchange between the surface and the gas is zero for a fully specular surface.

Because of the uncertainty in experimentally measured values for a_c^* , DSMC simulations were used to investigate the sensitivity of wire heat transfer to variations in a_c . Simulations were performed using different a_c values. Figure 8 shows the dependence of Nu_f on a_c for four different Kn_f cases. Results shown correspond to $U_\infty = 3$ m/s, though this same data was also produced for $U_\infty = 1, 8, 15,$ and 20 m/s. Similar trends are observed at other velocities. Only one case is presented for brevity. The simulated mixture is air (80% N_2 and 20% O_2) at various pressures ($P = 105, 300, 600,$ and 1000 Pa). Free-stream and wire temperatures are $T_\infty = 300$ K and $T_w = 373$ K. Wire diameter d is $20 \mu\text{m}$. The data shown for each value of Kn_f is quite linear for $a_c > 0.25$. It is known that all of these curves, however, must pass through the origin ($Nu_f = 0$ when $a_c = 0$) where all reflections are specular. This means that the gradient ($\partial Nu_f / \partial a_c$) must be very high and non-linear as a_c approaches zero. Details of the behaviour near $a_c = 0$ are not of particular interest to the current study because realistic values of a_c^* for hotwires are greater than 0.5, where the data appear linear. Results for heat transfer dependence on accommodation coefficient are used in the following section to visualize DSMC uncertainty due to uncertainty in values for a_c .

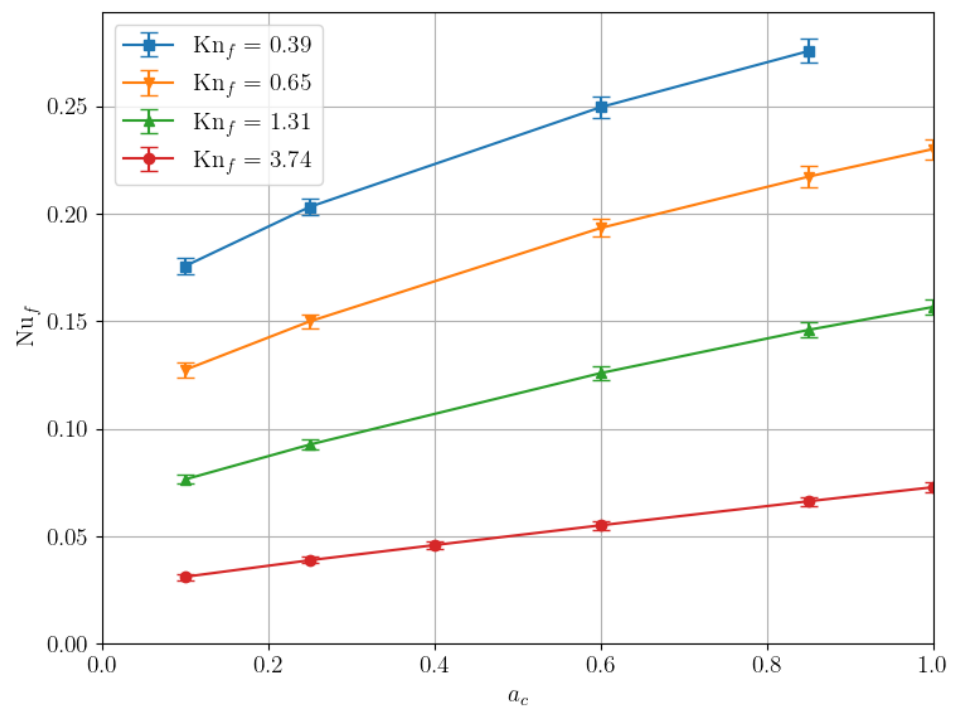


Figure 8. Dependence of wire heat transfer on surface accommodation coefficient at different values of wire Knudsen number. Data shown correspond to $U_\infty = 3$ m/s. Error bars indicate $\pm 1\sigma$ of the steady-state DSMC data.

3.4. Comparison with Experimental Data

An important practical goal of the current research is to use DSMC to supplement or replace experimental calibration of fine-wire anemometers. This requires that DSMC accurately predicts the relationship between Nu and Re . Figure 9 compares DSMC results and experimental data for Nu_f vs Re_f at different values of Kn_f [6]. Details of these simulations are the same as those presented in the previous section. Values for Kn_f are slightly different between the DSMC and experiment because pressure between comparing sets of data match, but there is a slight difference in gas composition. Experimental data is for pure N_2 , while simulations are run with two-species air. DSMC data presented use

$a_c = 0.85$, an estimate for tungsten wires in N_2 or O_2 [37]. Shaded regions surrounding the simulation results show uncertainty in Nu_f due to a $\pm 10\%$ uncertainty in a_c . This was computed by

$$\delta Nu_f = \frac{\partial Nu_f}{\partial a_c} \delta a_c \tag{13}$$

where δNu_f is the change in Nu_f due to changes in a_c (δa_c). At a given Re_f and Kn_f condition, several simulations were run, each with a different values of a_c (see Section 3.3). This data was used to estimate the derivative, $\partial Nu_f / \partial a_c$, at $a_c = 0.85$. Figure 8 shows a linear dependence of Nu_f on a_c near $a_c = 0.85$. This justifies a simple finite difference estimate of the derivative. Table 3 gives the average uncertainty in Nusselt number due to a 10% uncertainty in a_c for each of the four Knudsen number conditions.

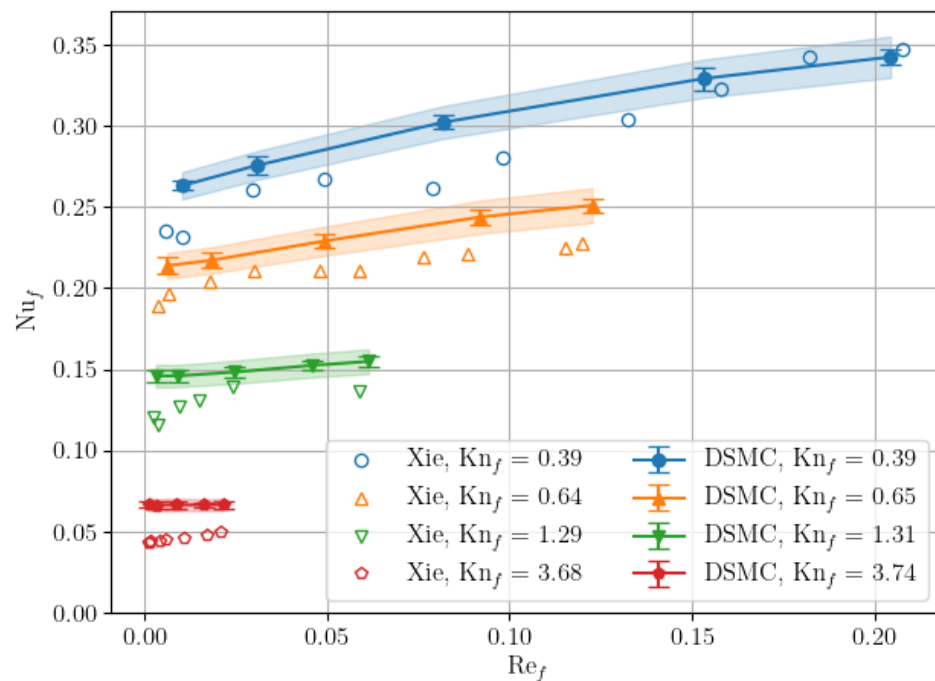


Figure 9. Comparison between DSMC results and experimental data [6]. Error bars indicate $\pm 1\sigma$ of the steady-state DSMC data. Shaded regions are predicted uncertainty bounds in the DSMC results due to a $\pm 10\%$ uncertainty in surface accommodation coefficient a_c .

Table 3. Average uncertainty in DSMC Nu_f due to a 10% uncertainty in a_c for the four different Knudsen cases seen in Figure 9.

Kn_f	$100 \times \frac{\delta Nu_f}{Nu_f}$
0.39	3.4%
0.65	4.0%
1.31	4.8%
3.74	5.7%

Results in Figure 9 show good agreement between DSMC and experiment, especially for low Kn_f , high Re_f cases. As could be expected from the study of heat transfer dependence on domain size in Section 2.3, the simulated heat transfer generally over-predicts the experimental data. The only region this is not the case is where Re_f is highest. For these cases, heat transfer due to forced convection is large relative to conduction between the wire and domain boundaries, minimizing finite domain effects. The approximate difference between the experimental and DSMC data (relative to the DSMC data) is 3%, 8%, 10%, and 30% for DSMC Kn_f values of 0.39, 0.65, 1.31, and 3.74, respectively.

It is evident, especially for the higher Kn cases, that the DSMC becomes less sensitivity to changes in Re_f as Re_f approaches zero. Experimental data shows the opposite trend with the Nu_f versus Re_f slope increasing at lower Re_f . It is hypothesized that finite domain size is the main cause of this behavior. At low Re_f , the convective heat transfer is very low, and the conduction through the fluid becomes important. The presence of the boundary is the main driver of the conductive heat transfer because it establishes a fixed distance between the wire and the free-stream over which the simulation can establish a temperature gradient. These results are consistent with those of Xie et al. [7] who showed that larger domains are required for lower values of Re. In light of this, an optimal simulation scheme would involve an inverse scaling of domain size with Re.

Simulation sensitivity at low Re_f is noticeably dependent on Kn_f , with higher Kn_f cases being less sensitive to Re_f than lower Kn_f cases. This is most noticeable when comparing the low Re_f results for the $Kn_f = 0.39$ and 3.74 cases. Over a similar Re_f range, a clear change in Nu_f is observed for $Kn_f = 0.39$ while no noticeable change is observed for $Kn_f = 3.74$. These data suggest that for a given Re_f , the required domain size of the simulation will increase with Kn_f . For CFD simulations in the slip-flow regime, Xie et al. [7] showed a very weak relationship between Kn and domain size for a given Re value. Current data suggests this dependence is stronger in the transition-regime, and the required domain size will scale with Kn_f . This behavior is reasonable when considering the communication of information between the domain boundary and the wire surface. Information in a gas is communicated by colliding molecules. At the low Kn values in the slip and continuum regimes, the number of collisions is sufficiently high such that thermal temperature of incident particles gradually changes from the free-stream (domain boundary) to near the surface temperature. At larger Knudsen number values, a finite number of collisions occur between the domain boundary and the wire surface. This will result in particles incident on the wire surface to have thermal energies closer to that of the free-stream than the lower Knudsen number case. If the domain boundary is too close to the wire, particles incident on the wire surface will have an artificially low thermal temperature ($T_\infty < T_w$) because they will experience an artificially low number of collisions. This will increase the energy transfer from the wire surface to incident gas particles. This will also decrease simulation sensitivity to free-stream velocity changes because conductive heat transfer will be artificially high relative to the convective heat transfer.

This reasoning explains why low sensitivity of Nu_f with Re_f is observed at low Re_f values and high Kn_f values. It also explains why simulations consistently over predict the wire heat transfer at these conditions. Optimal DSMC simulation domain size will scale proportionally with Kn and inversely with Re. This will result in the largest domain size for low Re and high Kn, and the smallest domain size at high Re and low Kn. This knowledge will help improve accuracy and efficiency of simulations for future studies.

To investigate the magnitude of the finite domain size effect on the results of Figure 9, one low Reynolds number condition was tested with increasing domain sizes. Results are shown in Figure 10. Wire Kn_f is 3.74, and free-stream velocity is 3 m/s ($Re_f = 0.0032$). The $L/d = 100$ case is the same data shown in Figure 9. The experimental data point from Xie et al. [6] that most closely matches the Kn_f and Re_f values is also shown ($Kn_f = 3.68$, $Re_f = 0.0038$). As domain size increases, the predicted heat transfer approaches the experimental value, but does not converge to the experimental value shown. Between a domain size of $L/d = 100$ and $L/d = 800$, simulated Nu_f dropped by 5.84%. While the above analysis can explain the trend differences between simulation and experiment, Figure 10 data suggest that the magnitude of the difference between simulation and experiment cannot be fully explained by finite simulation domain size. The remaining discrepancy between simulation and experiment may be due to differences in experimental and simulated conditions.

Future DSMC studies will further investigate the finite domain size problem that the current study has shown to be very important for these flows. Parametric studies

of pressure, free-stream temperature, wire temperature, and other variables will help to explain the likely cause of differences between simulation and experiment.

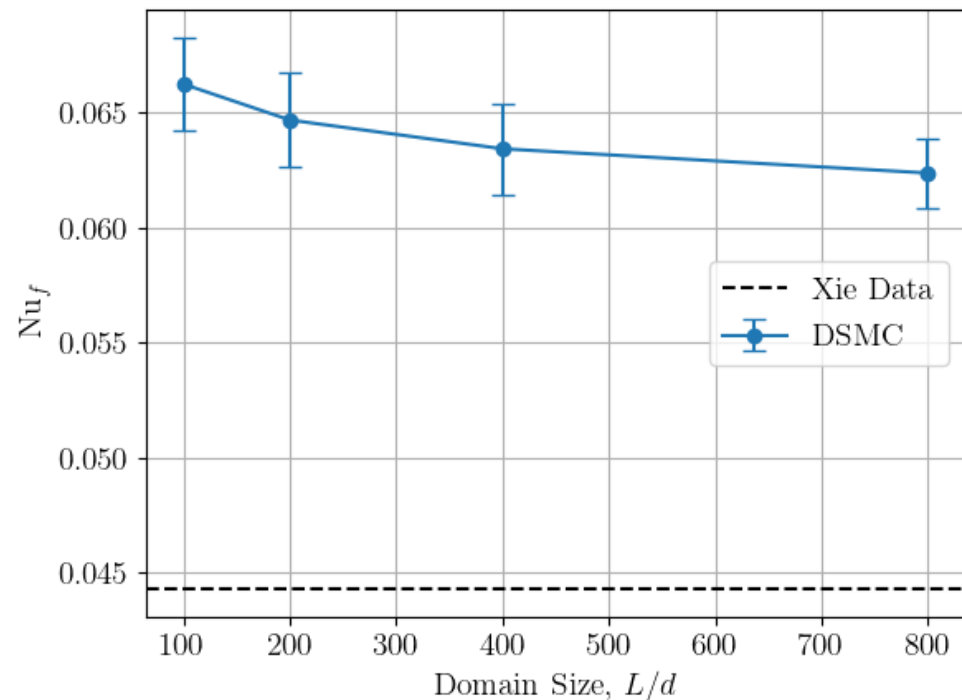


Figure 10. Simulated wire heat transfer dependence on domain size for the $Kn_f = 3.74$, $Re_f = 0.0032$ case. Error bars indicate $\pm 1\sigma$ of the steady-state DSMC data. The experimental value from Xie et al. [6] for $Kn_f = 3.68$, $Re_f = 0.0038$ is also shown.

4. Conclusions

The current article presents DSMC simulations of hotwire anemometers in the transition-regime. Results will aid in calibrating hotwire anemometers for in-situ turbulence measurements at high altitudes. Challenges associated with simulating these instruments are discussed. Dependence of heat transfer on accommodation coefficient is explored, and the results are used to show uncertainty in DSMC heat transfer due to uncertainty in accommodation coefficient. Comparison between simulation results and experimental data proves that the DSMC method can be used for accurately simulating low-speed hotwire anemometers at high-altitude conditions. Discrepancies in magnitude are attributed to differences in simulation and experimental conditions. Discrepancies in trend are attributed to finite simulation domain size. It is concluded that DSMC simulation domain size should scale proportionally with Kn and inversely with Re in order to efficiently reduce the error caused by a finite domain size.

Author Contributions: Writing—original draft, C.A.R.; Writing—review & editing, B.M.A. All authors have read and agreed to the published version of the manuscript.

Funding: Funding for this work comes from the Air Force Office of Scientific Research (AFOSR) grant FA9550-18-1-0009.

Acknowledgments: The authors would like to acknowledge Joseph L. Pointer and Dale A. Lawrence for the useful discussions that helped guide this research. This work utilized resources from the University of Colorado Boulder Research Computing Group, which is supported by the National Science Foundation (awards ACI-1532235 and ACI-1532236), the University of Colorado Boulder, and Colorado State University.

Conflicts of Interest: The authors declare no conflict of interest.

References

1. King, L.V., XII. On the convection of heat from small cylinders in a stream of fluid: Determination of the convection constants of small platinum wires with applications to hot-wire anemometry. *Philos. Trans. R. Soc. London. Ser. A Contain. Pap. A Math. Phys. Character* **1914**, *214*, 373–432. [\[CrossRef\]](#)
2. Collis, D.C.; Williams, M.J. Two-dimensional convection from heated wires at low Reynolds numbers. *J. Fluid Mech.* **1959**, *6*, 357. [\[CrossRef\]](#)
3. Levey, H.C. Heat transfer in slip flow at low Reynolds number. *J. Fluid Mech.* **1959**, *6*, 385. [\[CrossRef\]](#)
4. Kassoy, D.R. Heat Transfer from Circular Cylinders at Low Reynolds Numbers. I. Theory for Variable Property Flow. *Phys. Fluids* **1967**, *10*, 938. [\[CrossRef\]](#)
5. Andrews, G.; Bradley, D.; Hundy, G. Hot wire anemometer calibration for measurements of small gas velocities. *Int. J. Heat Mass Transf.* **1972**, *15*, 1765–1786. [\[CrossRef\]](#)
6. Xie, F.; Li, Y.; Liu, Z.; Wang, X.; Wang, L. A forced convection heat transfer correlation of rarefied gases cross-flowing over a circular cylinder. *Exp. Therm. Fluid Sci.* **2017**, *80*, 327–336. [\[CrossRef\]](#)
7. Xie, F.; Li, Y.; Wang, X.; Wang, Y.; Lei, G.; Xing, K. Numerical study on flow and heat transfer characteristics of low pressure gas in slip flow regime. *Int. J. Therm. Sci.* **2018**, *124*, 131–145. [\[CrossRef\]](#)
8. Deissler, R. An analysis of second-order slip flow and temperature-jump boundary conditions for rarefied gases. *Int. J. Heat Mass Transf.* **1964**, *7*, 681–694. [\[CrossRef\]](#)
9. Karniadakis, G.E. Numerical simulation of forced convection heat transfer from a cylinder in crossflow. *Int. J. Heat Mass Transf.* **1988**, *31*, 107–118. [\[CrossRef\]](#)
10. Lange, C.; Durst, F.; Breuer, M. Momentum and heat transfer from cylinders in laminar crossflow at $10^{-4} \leq \text{Re} \leq 200$. *Int. J. Heat Mass Transf.* **1998**, *41*, 3409–3430. [\[CrossRef\]](#)
11. Bharti, R.P.; Chhabra, R.P.; Eswaran, V. A numerical study of the steady forced convection heat transfer from an unconfined circular cylinder. *Heat Mass Transf.* **2006**, *43*, 639–648. [\[CrossRef\]](#)
12. Çelenligil, M.C. Heat transfer simulation of rarefied laminar flow past a circular cylinder. In *AIP Conference Proceedings*; AIP: Melville, NY, USA, 2016. [\[CrossRef\]](#)
13. Bird, G. *Molecular Gas Dynamics and the Direct Simulation of Gas Flows*; Oxford University Press: Oxford, UK, 1994.
14. Plimpton, S.J.; Moore, S.G.; Borner, A.; Stagg, A.K.; Koehler, T.P.; Torczynski, J.R.; Gallis, M.A. Direct simulation Monte Carlo on petaflop supercomputers and beyond. *Phys. Fluids* **2019**, *31*, 086101. [\[CrossRef\]](#)
15. U.S. Standard Atmosphere. *Technical Report NASA-TM-X-74335*; National Aeronautics and Space Administration: Washington, DC, USA, 1976.
16. Pilinski, M.D.; Argrow, B.M.; Palo, S.E. Drag Coefficients of Satellites with Concave Geometries: Comparing Models and Observations. *J. Spacecr. Rocket.* **2011**, *48*, 312–325. [\[CrossRef\]](#)
17. Sohn, I.; Li, Z.; Levin, D.A.; Modest, M.F. Coupled DSMC-PMC Radiation Simulations of a Hypersonic Reentry. *J. Thermophys. Heat Transf.* **2012**, *26*, 22–35. [\[CrossRef\]](#)
18. Liou, W.; Fang, Y. Heat transfer in microchannel devices using DSMC. *J. Microelectromech. Syst.* **2001**, *10*, 274–279. [\[CrossRef\]](#)
19. Cai, C.; Boyd, I.D.; Fan, J.; Candler, G.V. Direct Simulation Methods for Low-Speed Microchannel Flows. *J. Thermophys. Heat Transf.* **2000**, *14*, 368–378. [\[CrossRef\]](#)
20. Fang, Y.; Liou, W.W. Computations of the Flow and Heat Transfer in Microdevices Using DSMC With Implicit Boundary Conditions. *J. Heat Transf.* **2001**, *124*, 338–345. [\[CrossRef\]](#)
21. Fan, J.; Shen, C. Statistical Simulation of Low-Speed Rarefied Gas Flows. *J. Comput. Phys.* **2001**, *167*, 393–412. [\[CrossRef\]](#)
22. Sun, Q. Development of an information preservation method for subsonic, micro-scale gas flows. In *AIP Conference Proceedings*; AIP: Melville, NY, USA, 2001. [\[CrossRef\]](#)
23. Mahdavi, A.M.; Le, N.T.P.; Roohi, E.; White, C. Thermal Rarefied Gas Flow Investigations Through Micro-/Nano-Backward-Facing Step: Comparison of DSMC and CFD Subject to Hybrid Slip and Jump Boundary Conditions. *Numer. Heat Transf. Part A Appl.* **2014**, *66*, 733–755. [\[CrossRef\]](#)
24. Amiri-Jaghargh, A.; Roohi, E.; Niazmand, H.; Stefanov, S. DSMC Simulation of Low Knudsen Micro/Nanoflows Using Small Number of Particles per Cells. *J. Heat Transf.* **2013**, *135*. [\[CrossRef\]](#)
25. Stern, E.; Nompelis, I.; Schwartzentruber, T.E.; Candler, G.V. Microscale Simulations of Porous TPS Materials: Application to Permeability. In Proceedings of the 11th AIAA/ASME Joint Thermophysics and Heat Transfer Conference, Atlanta, GA, USA, 16–20 June 2014; American Institute of Aeronautics and Astronautics: Reston, VA, USA, 2014. [\[CrossRef\]](#)
26. Plotnikov, M.Y. Hydrogen Dissociation in Rarefied Gas Flow Through a Wire Obstacle. *J. Appl. Mech. Tech. Phys.* **2018**, *59*, 794–800. [\[CrossRef\]](#)
27. Stern, E.C.; Poovathingal, S.; Nompelis, I.; Schwartzentruber, T.E.; Candler, G.V. Nonequilibrium flow through porous thermal protection materials, Part I: Numerical methods. *J. Comput. Phys.* **2019**, *380*, 408–426. [\[CrossRef\]](#)
28. Poovathingal, S.; Stern, E.C.; Nompelis, I.; Schwartzentruber, T.E.; Candler, G.V. Nonequilibrium flow through porous thermal protection materials, Part II: Oxidation and pyrolysis. *J. Comput. Phys.* **2019**, *380*, 427–441. [\[CrossRef\]](#)
29. Çelenligil, M.C. *Numerical Simulation of Rarefied Laminar Flow Past a Circular Cylinder*; AIP Publishing LLC: Melville, NY, USA, 2014. [\[CrossRef\]](#)

30. Gu, X.J.; Barber, R.W.; John, B.; Emerson, D.R. Non-equilibrium effects on flow past a circular cylinder in the slip and early transition regime. *J. Fluid Mech.* **2018**, *860*, 654–681. [[CrossRef](#)]
31. Tseng, K.; Kuo, T.; Lin, S.; Su, C.; Wu, J. Simulations of subsonic vortex-shedding flow past a 2D vertical plate in the near-continuum regime by the parallelized DSMC code. *Comput. Phys. Commun.* **2012**, *183*, 1596–1608. [[CrossRef](#)]
32. Ikegawa, M.; Kobayashi, J. Development of a Rarefield Gas Flow Simulator Using the Direct-Simulation Monte Carlo Method: 2-D Flow Analysis with the Pressure Conditions Given at the Upstream and Downstream Boundaries. *JSME Int. J.* **1990**, *33*, 463–467. [[CrossRef](#)]
33. Nance, R.P.; Hash, D.B.; Hassan, H.A. Role of Boundary Conditions in Monte Carlo Simulation of Microelectromechanical Systems. *J. Thermophys. Heat Transf.* **1998**, *12*, 447–449. [[CrossRef](#)]
34. Piekos, E.; Breuer, K. DSMC modeling of micromechanical devices. In *Proceedings of the 30th Thermophysics Conference, San Diego, CA, USA, 19–22 June 1995*; American Institute of Aeronautics and Astronautics: Reston, VA, USA, 1995. [[CrossRef](#)]
35. Sun, H.; Faghri, M. Effects of Rarefaction and Compressibility of Gaseous Flow in Microchannel Using DSMC. *Numer. Heat Transf. Part A Appl.* **2000**, *38*, 153–168. [[CrossRef](#)]
36. Shah, N.; Gavasane, A.; Agrawal, A.; Bhandarkar, U. Comparison of Various Pressure Based Boundary Conditions for Three-Dimensional Subsonic DSMC Simulation. *J. Fluids Eng.* **2017**, *140*. [[CrossRef](#)]
37. Amdur, I.; Guildner, L.A. Thermal Accommodation Coefficients on Gas-covered Tungsten, Nickel and Platinum1. *J. Am. Chem. Soc.* **1957**, *79*, 311–315. [[CrossRef](#)]
38. Goodman, F. Thermal accommodation. *Prog. Surf. Sci.* **1974**, *5*, 261–375. [[CrossRef](#)]
39. Chen, S.; Saxena, S. Interface heat transfer and thermal accommodation coefficients: Heated tungsten wire in nitrogen environment. *Int. J. Heat Mass Transf.* **1974**, *17*, 185–196. [[CrossRef](#)]